Optical Investigation of Broadband White-Light Emission in Self-Assembled Organic-Inorganic Perovskite (C6H11NH3)2PbBr4

ARTICLE *in* THE JOURNAL OF PHYSICAL CHEMISTRY C · SEPTEMBER 2015

Impact Factor: 4.77 · DOI: 10.1021/acs.jpcc.5b06211

12 AUTHORS, INCLUDING:

Jean-Sébastien Lauret

Ecole normale supérieure de Cachan

144 PUBLICATIONS **1,597** CITATIONS

SEE PROFILE

Sébastien Pillet

University of Lorraine

50 PUBLICATIONS **431** CITATIONS

SEE PROFILE

Smail Triki

Université de Bretagne Occidentale

124 PUBLICATIONS **2,184** CITATIONS

SEE PROFILE

Younes Abid

University of Sfax

78 PUBLICATIONS **515** CITATIONS

SEE PROFILE

THE JOURNAL OF PHYSICAL CHEMISTRY C

Article

pubs.acs.org/JPCC

Optical Investigation of Broadband White-Light Emission in Self-Assembled Organic–Inorganic Perovskite $(C_6H_{11}NH_3)_2PbBr_4$

A. Yangui,[†,‡] D. Garrot,[*,†] J. S. Lauret,[§] A. Lusson,[†] G. Bouchez,[†] E. Deleporte,[§] S. Pillet,[∥] E. E. Bendeif,[∥] M. Castro,[⊥] S. Triki,[#] Y. Abid,[‡] and K. Boukheddaden[*,†]

[†]Groupe d'Etudes de la Matière Condensée (GEMaC), CNRS, Université de Versailles Saint-Quentin-en-Yvelines, 45 Avenue des Etats-Unis, 78035 Versailles Cedex, France

[‡]Laboratoire de Physique Appliquée (LPA), Faculté des Sciences de Sfax, Route de Soukra km 3.5 BP 1171, 3018 Sfax, Tunisia

[§]Laboratoire Aimé Cotton, Ecole Normale Supérieure de Cachan, CNRS, Université de Paris-Sud, Bât 505 Campus d'Orsay, 91405 Orsay, France

[∥]Université de Lorraine, CRM2, UMR 7036, F-54506 Vandoeuvre-les-Nancy, France

[⊥]Departamento de Ciencia y Tecnología de Materiales y Fluidos, Escuela de Ingeniería y Arquitectura, Instituto de Ciencia de Materiales de Aragón (CSIC-Universidad de Zaragoza), C/Maria de Luna no. 3, 500018 Zaragoza, Spain

[#]Laboratoire de Chimie, Electrochimie Moléculaires et Chimie Analytique, CNRS, Université de Bretagne Occidentale, BP 809, 29285 Brest, France

Supporting Information

ABSTRACT: The performance of hybrid organic perovskite (HOP) for solar energy conversion is driving a renewed interest in their light emitting properties. The recent observation of broad visible emission in layered HOP highlights their potential as white-light emitters. Improvement of the efficiency of the material requires a better understanding of its photophysical properties. We present in-depth experimental investigations of white-light (WL) emission in thin films of the $(C_6H_{11}NH_3)_2PbBr_4$. The broadband, strongly Stokes shifted emission presents a maximum at 90 K when excited at 3.815 eV, and below this temperature coexists with an excitonic edge emission. X-rays and calorimetry measurements exclude the existence of a phase transition as an origin of the thermal behavior of the WL luminescence. The free excitonic emission quenches at low temperature, despite a binding energy estimated to 280 meV. Time-resolved photoluminescence spectroscopy reveals the multicomponent nature of the broad emission. We analyzed the dependence of these components as a function of temperature and excitation energy. The results are consistent with the existence of self-trapped states. The quenching of the free exciton and the thermal evolution of the WL luminescence decay time are explained by the existence of an energy barrier against self-trapping, estimated to ∼10 meV.

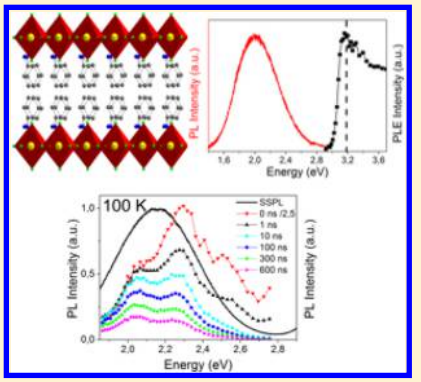

I. INTRODUCTION

During the last decades, great attention has been devoted to the large family of hybrid organic perovskites (HOP) due to their special structural features and their important optical properties. These materials are known to crystallize in zero-, one-, two, or three-dimensional structures.[1,2] The 3D HOP have drawn considerable attention since 2012 for their application in photovoltaic devices.[3−6] In particular, $CH_3NH_3PbI_3$ and its derivatives present exceptional potential for the fabrication of hybrid solar cells with efficiencies approaching 20%.[7] Recently, amplified spontaneous emission has also been reported, which makes these materials attractive candidates for the realization of on-chip coherent light source.[8] Their 2D counterparts have the general chemical formula $(R{-}NH_3)_2MX_4$ or $(H_3N{-}R{-}NH_3)$-MX_4, where R is an organic group, M a divalent metal, and X a halogen. They can be easily deposited as thin films by the spin-coating technique and self-assembled in a multiquantum well structure.[1,9] The carriers are confined in the inorganic part formed by MX_6 octahedra, and the organic part acts like a potential barrier (Figure 1). Besides, the high dielectric contrast between the organic and inorganic part contributes to strengthen the 2D confinement by image charge effect.[10] These mechanisms lead to the existence of excitons with large binding energy of a few hundred meV.[11,12] 2D HOP exhibit strong photoluminescence[12] and electroluminescence,[13−15] even at room temperature, which makes them legitimate candidates for an integration in electronic and optoelectronic devices such as organic–inorganic light emitting diodes (OILED), field effect transistors, or polariton lasers.[12,13,15−17] In addition, the electronic and optical properties of 2D HOP can be controlled through chemical engineering of the organic part.[18−20] On the contrary, the choice of the organic part for

Received: June 29, 2015
Revised: September 9, 2015

DOI: 10.1021/acs.jpcc.5b06211
J. Phys. Chem. C XXXX, XXX, XXX−XXX

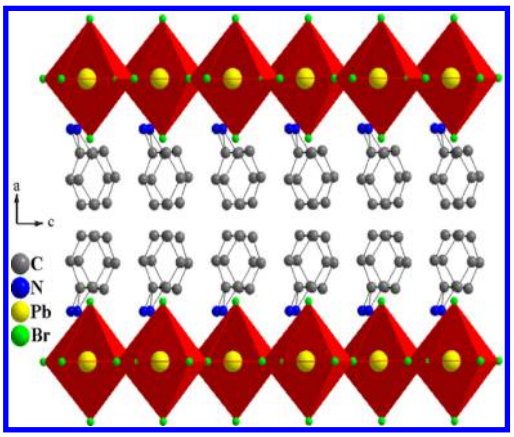

Figure 1. Sketch of the X-ray diffraction structure of $(C_6H_{11}NH_3)_2PbBr_4$ single crystal.

3D HOP is limited because the molecule has to be small enough to maintain the 3D structure.

Very recently, Dohner et al.[21,22] have observed white-light emission under UV irradiation in two families of hybrid perovskites, (*N*-MEDA)$PbBr_{4-x}Cl_x$ (*N*-MEDA = N^1-methyl-ethane-1,2-diammonium) and (EDBE)PbX_4 (EDBE = 2,2′-(ethylenedioxy)bis(ethylammonium)) with X = Cl or Br. The chromaticity of the emission was partially tuned with the choice of the halogen, and a stable photoluminescence quantum efficiency (PLQE) of 9% has been measured. These results highlight the great potential of these materials as white-light emitters.

However, the physical origin of this phenomenon is still uncertain. A better understanding of its photophysical properties and the possibility of chemical engineering should lead to the design of material with improved PLQE. We report here on the optical properties of a broad white-light emission in the 2D HOP $(C_6H_{11}NH_3)_2PbBr_4$, under UV irradiation. This Article is organized as follows: section II details the experimental methods used in the present study; section III is devoted to the experimental results and their interpretation; and in section IV we conclude.

II. EXPERIMENTAL METHODS

Synthesis. All reagents were purchased from commercial vendors and used as received. The purity of the products used is greater than 99%. Solvents were of reagent grade or higher purity. All manipulations were conducted in air. In a first step, the ammonium salt $C_6H_{11}NH_2$·HBr was prepared using the reaction between cyclohexylamine $C_6H_{11}NH_3$ and HBr (47 wt %) in the cold (−20 °C), to remove the reaction heat, with stirring for 20 min. Water was evaporated by elevating the temperature followed by washing with diethyl ether. The colorless precipitate was dried under vacuum. In a second step, 367 mg of $PbBr_2$ (1 mmol) in 2 mL of HBr (47 wt %) was added to 360 mg of $C_6H_{11}NH_2$·HBr and mixed in the methanol solvent, at room temperature. After 3 days, colorless platelets were formed.

Crystal Structure. A colorless single crystal of $(C_6H_{11}NH_3)_2PbBr_4$ with approximate dimensions 0.05 × 0.21 × 0.32 mm^3 was selected for the X-ray diffraction experiments. The X-ray data collection was carried out using a supernova 4-circle microsource diffractometer (Oxford Diffraction) equipped with a two-dimensional ATLAS detector, and using graphite monochromatized Mo Kα radiation (λ = 0.71073 Å). Data were collected at 293 K. The structure was solved by direct methods and successive Fourier difference syntheses, and was refined on F^2 by weighted anisotropic full-matrix least-squares methods using SHELX-2013 crystallographic software package.[23] All non-hydrogen atoms were refined anisotropically, while the hydrogen atoms were calculated and therefore included as isotropic fixed contributors to F_C. Data collection and data reduction were carried out using the CRYSALIS-CCD and CRYSALIS-RED programs.[24]

Single-crystal X-ray studies were collected at T = 20, 50, and 90 K on a Microfocus Supernova diffractometer equipped with a two-dimensional ATLAS detector, using Mo Kα radiation (λ = 0.71073 Å), and a Helijet He open flow cryosystem. Numerical absorption correction was performed according to the crystal faces. The corresponding structures were solved by direct methods with the SHELXS program and refined on F^2 by weighted full matrix least-squares methods using the SHELXL program. All non-hydrogen atoms were refined anisotropically, and hydrogen atoms were generated at their ideal positions and treated using a riding model. The ammonium cation exhibits severe disorder, which was treated using two configurations whose populations P1 and P2 were refined with the constraint P1 + P2 = 1.0. The disordered non hydrogen atoms of the ammonium cation were restricted to isotropic atomic displacement parameters and constrained to be equivalent for the two cation orientations.

Films. The thin films of $(C_6H_{11}NH_3)_2PbBr_4$ was prepared by spin-coating technique. The thickness was estimated to 300 nm with surface profilometry. Twenty milligrams of $(C_6H_{11}NH_3)_2PbBr_4$ crystal was dissolved in 1.1 mL of *N*−*N*-dimethylformamide (DMF) solvent and spin-coated on a quartz slide at 1500 rpm for 20 s. The film was then annealed at 80 °C for 30 min to remove residual solvent.

Calorimetry. Heat capacity was determined in the temperature range of 25−200 K by thermal relaxation calorimetry using the Quantum Design Physical Property Measurement System (PPMS). A few small crystals of $(C_6H_{11}NH_3)_2PbBr_4$, with a total mass of around 1 mg, were mounted by pressing them over a small amount of Apiezon N Grease applied as a layer onto the sample platform. The reported heat capacity data, after subtracting the contribution of the sample platform, correspond to the heat capacity of both the crystals and the Apiezon N Grease. Approximately, the sample contributes to around 40% and 7% of the total measured heat capacity (sample platform + Apiezon N grease + sample) at 20 and 180 K, respectively.

Optical Measurements. Absorption measurements were taken on the spin-coated film and deduced from direct transmission measurements performed using a conventional UV−visible spectrophotometer (HITACHI, U-3300). For the PLE measurement, the excitation source was a xenon arc lamp filtered with a monochromator. The photoluminescence spectra were recorded using a spectrapro 2500i spectrometer equipped with a Pixis: 100B CCD array detector (Ropers scientific). The excitation wavelength was the 325 nm (3.815 eV) line of a He−Cd laser. The sample was placed on the coldfinger of a helium closed cycle cryostat. Time-resolved photoluminescence was performed using the Time-Correlated Single Photon Counting TimeHarp 260 system from PicoQuant. The excitation was the second harmonic of a pulse from a Ti:sapphire laser (Mai Tai, Spectra-Physics). The emission was detected with a single photon avalanche diode (IDQuantique ID150). Repetition rate

DOI: 10.1021/acs.jpcc.5b06211
J. Phys. Chem. C XXXX, XXX, XXX−XXX

was adjusted thanks to a pulse picker (Spectra Physics) from 80 MHz to 80 kHz.

III. RESULTS AND DISCUSSION

$(C_6H_{11}NH_3)_2PbBr_4$ crystallizes in the orthorhombic system $Cmc2_1$ space group, with a primitive unit cell of dimensions a = 27.957(2) Å, b = 8.6288(6) Å, c = 8.3745(5) Å and four formula units (Z = 4), at room temperature. The relevant structural data are summarized in Table 1. The crystal structure shows a two-dimensional (2D) periodic arrangement of the inorganic layers formed by corner-sharing $PbBr_6$ octahedra and the organic layers $C_6H_{11}NH_3$ (Figure 1). The organic sheets of layered perovskites can be derived from the (100) crystallographic planes of the three-dimensional perovskite structure.

Table 1. Crystallographic Data for $(C_6H_{11}NH_3)_2PbBr_4$

empirical formula	$C_{12}H_{28}Br_4N_2Pb$
temperature, K	293
formula weight, g mol^{-1}	727.19
wavelength, Å	Mo Kα (λ = 0.71073 Å)
crystal system	orthorhombic
space group	$Cmc2_1$
a, Å	27.957(2)
b, Å	8.6288(6)
c, Å	8.3745(5)
volume, Å^3	2020.2(2)
Z	4
density (calculated), g cm^{-3}	2.39
absorption coefficient, mm^{-1}	16.255
F(000)	1344
crystal size, mm^3	0.05 × 0.21 × 0.32
crystal color/shape	colorless/platelets
maximum 2θ, deg	56.56
hkl range	h = −36/36, k = −11/9, l = −11/8
reflns collected/unique	12429/2305
data with $F_0 > 4\sigma(F_0)$	2097
highest peak/deepest hole, e Å^{-3}	0.867/−2.593
GOF	1.146
R_{int}	0.0521
R (σ)	0.0327
wR_2[a]	0.0864
R_1[b] (obs data)/R_1 (all data)	0.0368/0.0430

[a] $R_1 = \sum(|F_o - F_c|/F_o)$ and $wR_2 = [((\sum w(F_o^2 - F_c^2)^2)/(\sum(F_o^2)^2))]^{1/2}$. [b] G.O.F. $= [(\sum(\omega(F_o^2 - F_c^2))^2/(N_{obs} - N_{var})]^{1/2}$.

The absorption spectrum of the spin-coated thin film of $(C_6H_{11}NH_3)_2PbBr_4$ (Figure 2a) shows a behavior similar to those of other lead bromide hybrid perovskites[20,25−28] with a sharp excitonic absorption peaked at 3.19 eV and an absorption continuum at higher energy. The absorption band at 3.85 eV has been ascribed to interband transition.[12] Upon 325 nm (3.815 eV) excitation, $(C_6H_{11}NH_3)_2PbBr_4$ shows a very broad emission, structureless and Gaussian shaped, with a large Stokes shift (1.2 eV) that spans the entire visible spectrum, with a maximum intensity at 2 eV and a full width at half-maximum (FWHM) of 660 meV (Figure 2b). The excitation spectra (PLE) recorded with a detection energy of 2 eV coincide with the excitonic and the absorption continuum of the perovskite (Figure 2b).

At low temperature, the high energy emission spectrum presents two additional sharp excitonic peaks, located at 3.11 eV (Ex1) and 3.05 eV (Ex2) (Figure 3a). There are no detectable shifts of these emissions as a function of temperature. The peak at 3.11 eV is sharper than that at 3.05 eV with a FWHM of approximately 30 meV against 66 meV for Ex2 and has a small Stokes shift (less than 10 meV). The Ex1 and Ex2 emissions decrease quickly with temperature and are no more detectable above 90 K (Figure 3a). At higher temperature, the edge emission seems to disappear in the background of the WL emission. The coexistence of free and bound excitons is often observed in hybrid perovskites.[29] Excitons could be trapped by weak potential of lattice imperfections, such as defects, or structural disorder in general. Trapped excitons present a Stokes shift due to this potential minimum, which decreases at higher temperature and eventually disappears when the thermal energy exceeds the trapping potential. Therefore, we could consider Ex1 and Ex2 as free excitonic emission and shallow bound exciton, respectively. We described the quenching of Ex1 and Ex2 emission as due to a competition with a nonradiative channel as described by the familiar law:[30]

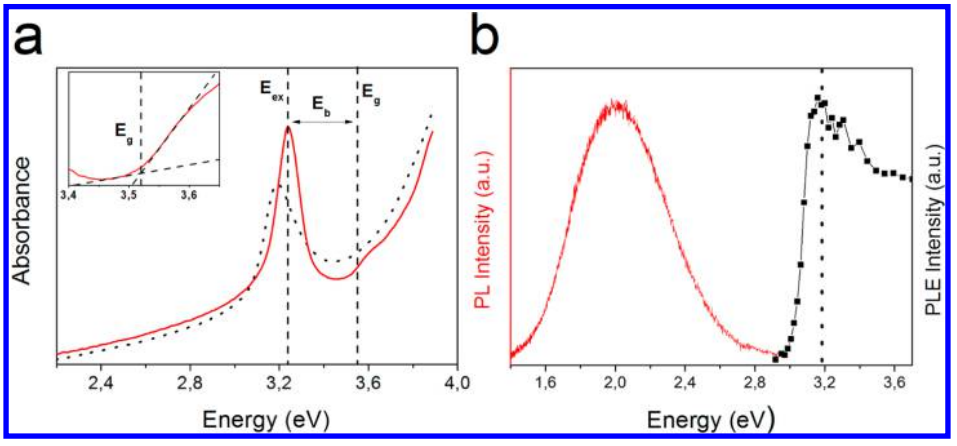

Figure 2. (a) Absorption spectra of $(C_6H_{11}NH_3)_2PbBr_4$ thin film measured at 300 K (dotted line) and 12 K (solid line). The inset shows the absorption spectrum at 12 K around the band edge. E_{ex}, E_g, and E_b represent the exciton energy, the energy gap, and the exciton binding energy, respectively. (b) Room-temperature photoluminescence with E_{excit} = 3.815 eV (red) and photoluminescence excitation measured at 2.05 eV (black) spectra for $(C_6H_{11}NH_3)_2PbBr_4$ thin film. The dotted line indicates the position of the excitonic absorption peak at room temperature.

DOI: 10.1021/acs.jpcc.5b06211
J. Phys. Chem. C XXXX, XXX, XXX−XXX

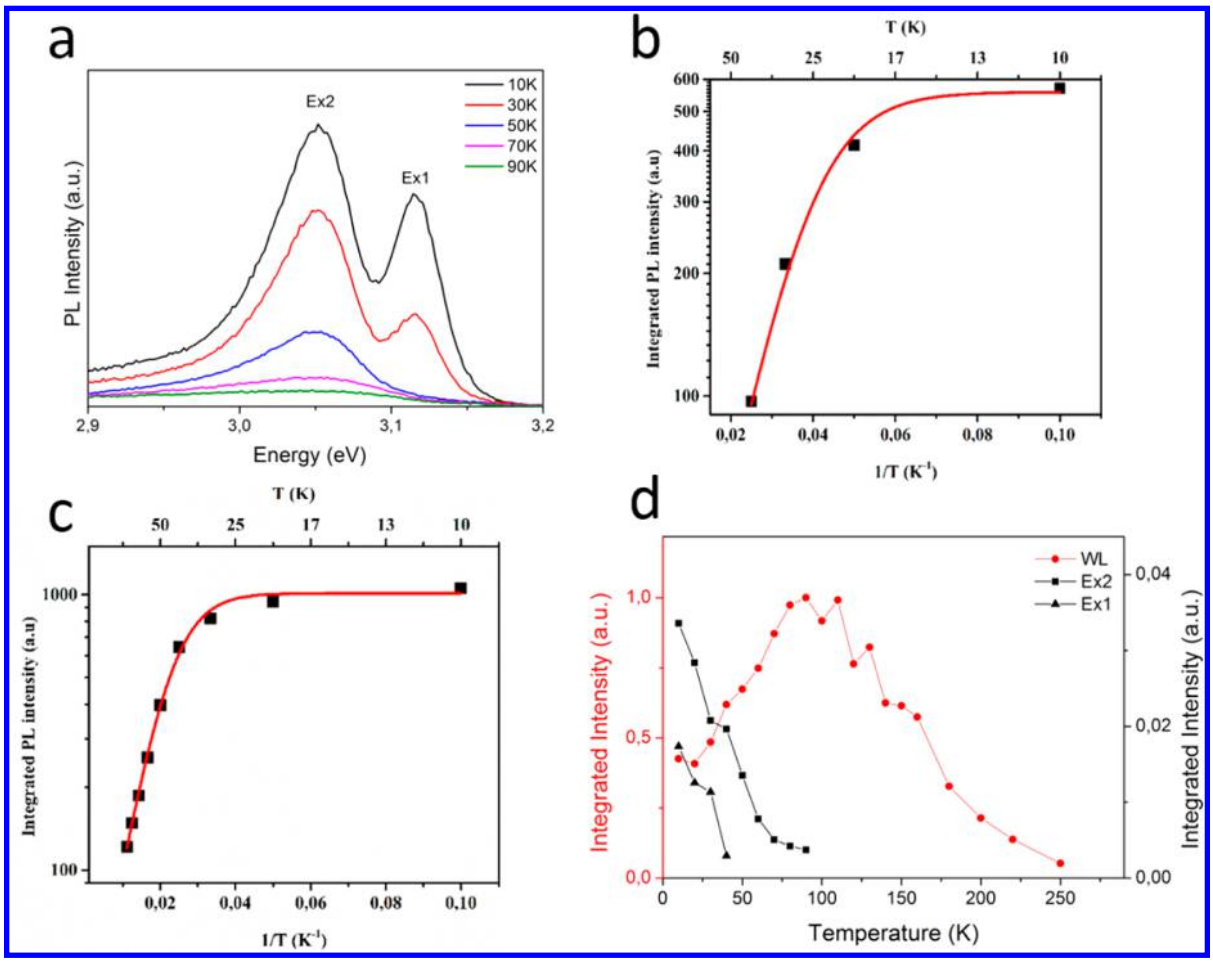

Figure 3. (a) PL spectra (E_{excit} = 3.81 eV) for temperatures ranging from 10 to 90 K for Ex1 and Ex2. (b) Refinement of the thermal dependence of PL intensity of Ex_1 using eq 1 with I_0 = 558 ± 20, a = 84.75 ± 9.6, and E_a = 9.86 ± 0.54 meV and (c) Ex_2 with I_0 = 1012.4 ± 32, a = 55.845 ± 4.93, and E_a = 14.93 ± 0.86 meV. (d) Thermal dependence of the integrated intensities of the Ex1, Ex2, and WL emission peaks.

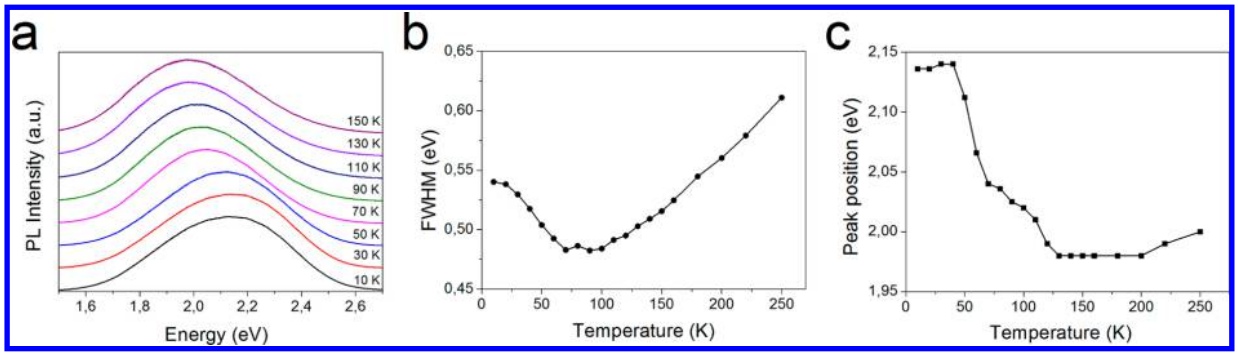

Figure 4. (a) Emission spectra between 10 and 150 K. Thermal evolution of the (b) FWHM and (c) peak position of the WL band under 3.815 eV excitation.

$$I = \frac{I_0}{1 + a \exp\left(-\frac{E_a}{k_B T}\right)} \quad (1)$$

where I_0 is the zero-temperature PL intensity, k_B is the Boltzmann constant, a is the ratio between the radiative and the nonradiative decay rates, and E_a is the activation energy. The best-refinement gives E_a = 9.86 ± 0.54 meV and E_a = 14.93 ± 0.86 meV for Ex1 and Ex2, respectively (Figure 3b and c). The exciton binding energy could be deduced from low-temperature absorption spectroscopy. Figure 2a shows the absorption spectrum of our film measured at 12 K. The step-like structure at 3.5 eV corresponds to the energy gap of the perovskite. An exciton binding energy of 280 meV is deduced from the difference between the excitonic peak and the band gap energies. This result is in good agreement with literature of $PbBr_4$ layered perovskites, where reported binding energies are in the range of several hundred meV: 200−300 meV for $(C_nH_{2n+1}NH_3)_2PbBr_4$ (n = 4, 5, 7, 12)[25] and 200 meV for $(C_6H_5C_2H_4NH_3)_2PbBr_4$,[29] for example. Consequently, the quenching of excitonic luminescence at low temperature could not correspond to the exciton dissociation.

DOI: 10.1021/acs.jpcc.5b06211
J. Phys. Chem. C XXXX, XXX, XXX−XXX

Table 2. Low-Temperature Crystallographic Data

	temp/K		
	20	50	90
chemical formula	$C_{12}H_{28}Br_4N_2Pb$	$C_{12}H_{28}Br_4N_2Pb$	$C_{12}H_{28}Br_4N_2Pb$
formula weight	727.19	727.19	727.19
crystal system	orthorhombic	orthorhombic	orthorhombic
space group	$Cmc2_1$	$Cmc2_1$	$Cmc2_1$
a/Å	27.4995(10)	27.6108(12)	27.6460(16)
b/Å	8.6281(3)	8.6324(4)	8.637(2)
c/Å	8.1775(3)	8.1958(4)	8.1913(10)
volume/Å^3	1940.26(12)	1953.45(16)	1955.9(5)
Z	4	4	4
ρ_{calc}, g/cm^3	2.489	2.473	2.470
μ/mm^{-1}	16.924	16.810	16.789
$F(000)$	1344	1344	1344
crystal size/mm^3	0.216 × 0.342 × 0.058	0.216 × 0.342 × 0.058	0.223 × 0.315 × 0.042
radiation	Mo Kα (λ = 0.71073)	Mo Kα (λ = 0.71073)	Mo Kα (λ = 0.71073)
maximum 2θ	56.56	56.56	56.56
hkl range	−36/27, −11/9, −9/10	−36/36, −11/11, −10/10	−36/36, −11/11, −10/10
collected reflns	5592	9574	9694
independent reflns	2163 [R_{int} = 0.055]	2477 [R_{int} = 0.029]	2232 [R_{int} = 0.032]
parameters/restraints	80/14	80/8	80/8
final R indexes[a]	R_1 = 0.036, wR_2 = 0.082	R_1 = 0.025, wR_2 = 0.053	R_1 = 0.032, wR_2 = 0.078
GOF[b] on F^2	1.097	1.044	1.138
largest diff. peak/hole/e Å^{-3}	1.67/−1.26	0.70/−1.25	1.09/−1.08

[a] $R1 = \sum(|F_o - F_c|/F_o)[I \geq 2\sigma(I)]$ and $wR_2 = [\sum((\omega(F_o^2 - F_c^2))^2/(\omega(F_o^2))^2)]^{1/2}$ [all data]. [b] $GOF = [(\sum(\omega(F_o^2 - F_c^2))^2/(N_{obs} - N_{var})]^{1/2}$.

Now, we focus on the nonmonotonous thermal behavior of the broad WL emission. The intensity of the WL emission excited at 3.815 eV increases with temperature, reaches a maximum at 100 K (Figure 3d), and then decreases. Above 100 K, the PL intensity decreases on heating as $\exp(E/k_BT)$ with E = 83 ± 3.7 meV. The increase of the PL intensity between 20 and 100 K seems to be correlated with the decrease of the Ex1 and Ex2 peaks (Figure 3d). Therefore, our results strongly suggest that the quenching of Ex1 and Ex2 in $(C_6H_{11}NH_3)_2PbBr_4$ could be attributed to the competition in the recombination process with the WL band.

A detailed inspection of the WL band shape shows a complex thermal evolution (Figure 4a). Indeed, the PL enhancement between 20 and 100 K is accompanied by a narrowing of the emission and a red shift of the peak position of approximately 150 meV (Figure 4b and c).

Hybrid organic−inorganic perovskites are known to present phase transitions, generally linked to the organic layer of the material.[31−33] These phase transitions could have an important impact on the optical properties and in particular could result in band gap switching in 2D and 3D HOP.[10,34,35]

We have investigated the possible existence of a phase transition in $(C_6H_{11}NH_3)PbBr_4$ at low temperature, which could be at the origin of the specific thermal behavior of the WL emission.

Single-crystal X-ray diffraction experiments were carried out at 20, 50, and 90 K to detect the presence of a possible structural phase transition in the 20−100 K temperature range. The details on the data collection and structural refinement are summarized in Table 2.

From 20 to 90 K, the unit cell parameters do not show any significant features, besides usual thermal expansion effects, the unit cell volume expanding regularly from 1940.3(1) to 1955.9(5) Å^3. No space group change was detected; the three structures were determined in the $Cmc2_1$ space group, in agreement with the structure reported at 173 K by Billing and Lemmerer.[36] As shown in Figure S1, the corresponding diffraction pattern does not exhibit any evidence for a structural phase transition with change of unit cell constants; neither were any superstructure reflections detected. By comparison with the results reported by Billing and Lemmerer, only gradual evolution of the structural parameters was observed (see Table S1), as the inorganic layer does not undergo any abrupt distortion. In addition, the ammonium cation does not exhibit any specific ordering, change of conformation, or change in N−H···Br hydrogen-bond network. Calorimetry measurements are also very important to assess the existence of a phase transition.[31−33]

The thermal dependence of the heat capacity (Figure 5) does not indicate the presence of any visible anomaly. Although these results do not allow one to definitely exclude the existence of small rearrangements and/or smooth second-order phase transitions, they clearly preclude the existence of any first-order phase transition at low temperature. In particular, in the temperature interval 10−100 K, where the thermal dependence of the PL showed the most significant variation, the heat capacity increases continuously following the usual trends of heat capacity of solids due to lattice phonons.

On the basis of the present crystallographic analysis and calorimetry measurements, the unusual thermal behavior of the WL emission could not be explained by the existence of a phase transition.

Another hypothesis is that the emission is in reality composed of different bands. To clarify this point, we performed time-resolved photoluminescence (TRPL) measurements as a function of temperature. Photoluminescence spectra at different delay show three distinct bands with maxima at 2.05, 2.29, and 2.5 eV, respectively (Figure 6). The narrow peak at 2.43 eV at 10 K is due to an unknown impurity of the substrate. The 2.5 eV band is short-lived and disappears on a

DOI: 10.1021/acs.jpcc.5b06211
J. Phys. Chem. C XXXX, XXX, XXX−XXX

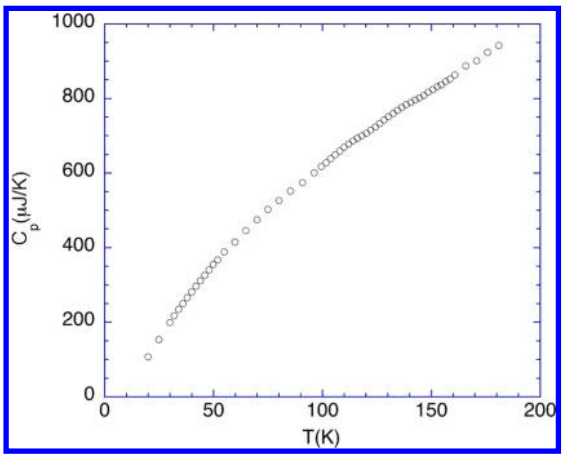

Figure 5. Thermal dependence of the heat capacity of $(C_6H_{11}NH_3)_2PbBr_4$ showing a continuous behavior excluding the existence of a first-order phase transition or a sharp second-order phase transition.

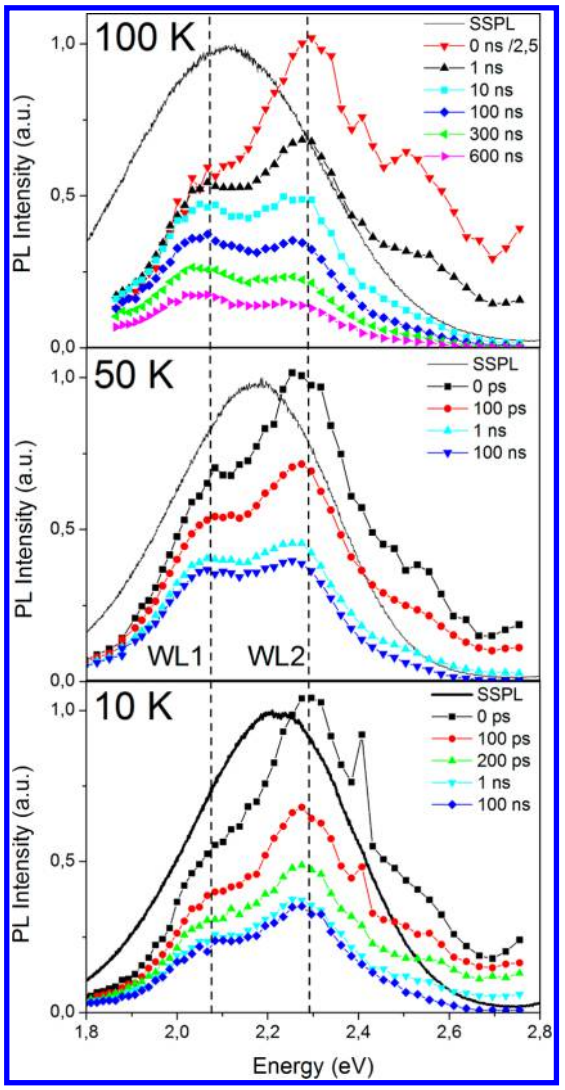

Figure 6. Steady-state and time-resolved photoluminescence spectra after excitation at 3.1 eV, at a temperature of 10, 50, and 100 K. Dashed lines indicate the position of the WL1 and WL2 bands. Note that, at 100K, the PL intensity of the spectrum at 0 ns is divided by a factor 2.5.

few nanoseconds time scale. The steady-state photoluminescence (SSPL) spectra (Figure 6) attest that its contribution to the overall emission is weak as compared to the two other bands. The already presented complex thermal evolution of the WL band between 10 and 100 K could be explained by the thermal behavior of the 2.05 eV (WL1) and 2.29 eV bands (WL2). First, we do not detect any measurable shift of these two bands as a function of temperature. However, at 10 K, the WL2 emission is more intense than WL1, and the overall emission maximum is at 2.22 eV. When the temperature is raised, the WL1 emission increases relatively to the other band, and the steady state spectra progressively red-shift to 2.15 eV at 100 K.

Because of the important overlapping of the two emissions and the similarity of their decay time scale, the exact shape and the specific lifetime of each band could not be properly separated. Both luminescence decays of WL1 and WL2 exhibited a fast component (Figure 7a), not resolved with our setup, and a slow exponential tail. The best fit of this "slow" component was obtained using a sum of two exponentials with time constants τ_1 and τ_2. The WL2 emission is dominant just after the excitation, at any temperature (Figure 6), due to its fast component. The slow luminescence decay in the high energy side of the WL emission, where WL2 is predominant, is also faster than that in the low energy side (Figure 7b). To study the thermal evolution of this slow component, we measured the luminescence decay of the WL emission, at the energy of its maximum. The temperature dependences of the decay times, τ_1 and τ_2, were derived using eq 2. The results, summarized in Figure 8, indicate that both constants undergo a significant decrease in the 10−100 K range.

The weight of the two bands in the overall emission depends on the temperature but also, and more surprisingly, on the excitation energy, especially at low temperature. WL emission excited at 3.815 eV (325 nm) (Figure 9a) is clearly red-shifted and broader than the emission excited at 3.1 eV (400 nm) (Figure 9b). We infer that WL1 band is more effectively excited when we use 3.815 eV excitation. Note that at 3.1 eV, we excite the edge of the excitonic absorption while the 3.815 eV excitation is in the energy continuum of the semiconductor. As we raise the temperature, the WL1 emission increases relatively to WL2, as previously stated, and the difference between the overall WL emission excited at 3.1 and 3.815 eV becomes less significant.

To go further, we studied the shape of the WL emission at different excitation energies at the same temperature (Figure 9c). As we increase the excitation energy, we clearly observe that the emission red-shifts and broadens. This result corroborates the hypothesis that the WL2 emission is excited preferentially at high excitation energy. By comparing Figure 9a with Figure 9c, the evolution of the shape of the emission as we raised the excitation energy seems close to that observed when we increase the temperature from 10 to 100 K, for the same excitation energy.

We discuss now the possible physical origin of this WL emission. We could consider two hypotheses. First, broad PL with important Stokes shift could result in the recombination of carriers localized at defects or impurities.[27,37] A strong coupling between the electronic states of the imperfection and the phonons of the crystal through the electron−phonon interaction could give rise to vibronics bands. In contrast with interband transition, the continuous spectral band of the imperfection comes from the coupling of the discrete electronic

DOI: 10.1021/acs.jpcc.5b06211
J. Phys. Chem. C XXXX, XXX, XXX−XXX

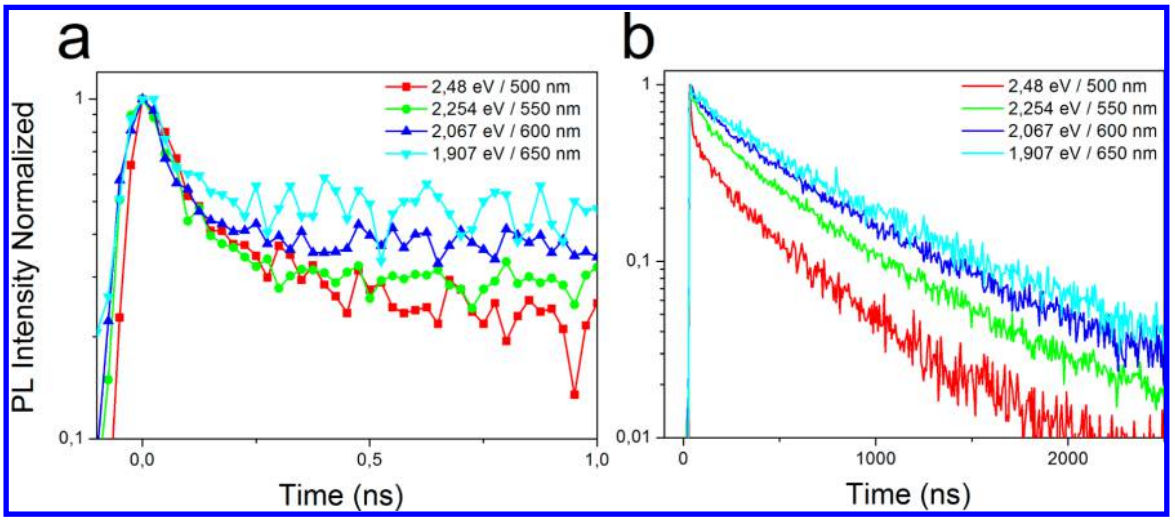

Figure 7. Normalized luminescence decay after excitation at 3.1 eV at 100 K at different energies, on 1 ns (a) and 2500 ns time scales (b).

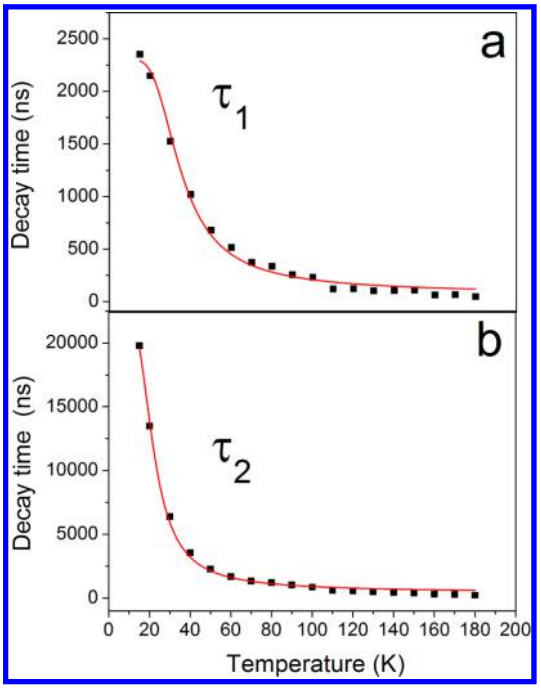

Figure 8. Temperature variation of the decay time constants obtained from the fit of the slow component with the sum of two exponentials. The experimental data are fitted with eq 2 (red line) with (a) E_1 = 11.5 meV, τ_0 = 2295 ns, υ = 0.017 ns; and (b) E_2 = 7.9 meV, τ_0 = 22.075 ns, and υ = 0.027 ns.

states to the phonons. The excited state is shifted as compared to the ground state by the electron−phonon interaction, measured by the Huang−Rhys factor. This shift is responsible for the energy difference between the absorption and the emission of the defect (Stokes shift), and also explains the width of the emission (Figure 10a). In fact, the carriers relax to the zero vibrational level of the ground state by emitting a photon and several phonons. Deep center defects lead to broad, Gaussian-shaped emission with a large Stokes shift as for the case of the yellow band in GaN.[27]

Second, self-trapping of excitons or electrons/holes also gives rise to broad-bands, Gaussian-shaped and strongly Stoke-shifted luminescence, which have been studied in alkali, ammonium, and lead halide.[38−41] Because of strong lattice coupling, charge carriers could be trapped in their own lattice distortion. In lead bromide, the recombination of self-trapped excitons and also of self-trapped holes with self-trapped electrons has been well studied.[42] The coexistence of free and self-trapped excitons has also been observed in alkali halide.[41,43] The mechanism of this coexistence could be described in a configuration coordinate diagram (Figure 10b). The conversion of a free exciton into a self-trapped exciton requires one to overcome a potential barrier by thermal activation or tunneling effect.[40] In some cases, excitons could also relax directly to the self-trapped state without passing through the bottom of the free-exciton band[38] (Figure 10b). The tunneling and the direct path should be relatively independent of temperature. The energy barrier E_B is linked to the elastic deformation required for the exciton localization. The presence of a permanent trap state could also help to localize the carrier when the electron−phonon coupling is not sufficient. In this case, an energy barrier could be observed between the defect and the self-trapped state. This situation is referred to as extrinsic self-trapping.[44]

We now consider the consistency of our results in the framework of these two hypothesis. First, permanent defect concentration and recombination lifetime are finite; thus their PL could be saturated at high excitation power.[27] However, the intensity of the WL luminescence presents a linear dependence with intensity up to 20 W/cm^2, as shown in Figure 11; the absence of saturation is in good agreement with the results of Dohner et al. on (*N*-MEDA)PbBr$_4$ and (EDBE)PbBr$_4$.[21,22] Above 20 W/cm^2 of excitation intensity, the photodegradation of the films unfortunately becomes non-negligible. The self-trapped carriers could be considered as transient defect states, and thus the absence of the saturation of the PL intensity with intensity is consistent with this hypothesis.

Concerning the thermal behavior of the emission, we observe that, below 20 K, the WL emission is nearly constant, and then in the 20−100 K range, it increases at the expense of the Ex1 and Ex2 emission. In classical semiconductors like GaN, the increase of defect related PL as the excitonic emission quenches is generally explained by the dissociation of the exciton and the redistribution of electrons/holes toward the defect. Yet in the case of $(C_6H_{11}NH_3)_2PbBr_4$, the binding energy is important, and we have discarded the possibility that the quenching of Ex1 and Ex2 at low temperature corresponds to the free exciton dissociation. Besides, the WL emission decreases drastically at

DOI: 10.1021/acs.jpcc.5b06211
J. Phys. Chem. C XXXX, XXX, XXX−XXX

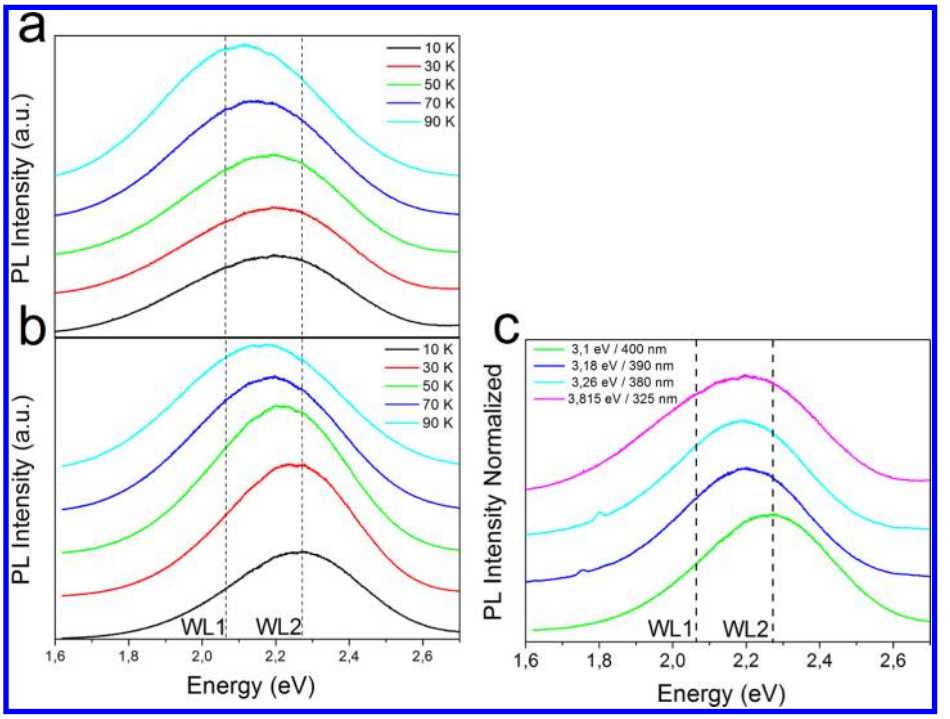

Figure 9. WL emission shape as a function of temperature and with excitation at (a) 3.851 eV (a) and (b) 3.1 eV. (c) WL emission spectra for different excitation energies at 10 K. Spectra are offset for clarity. Dashed lines indicate the position of the WL1 and WL2 bands.

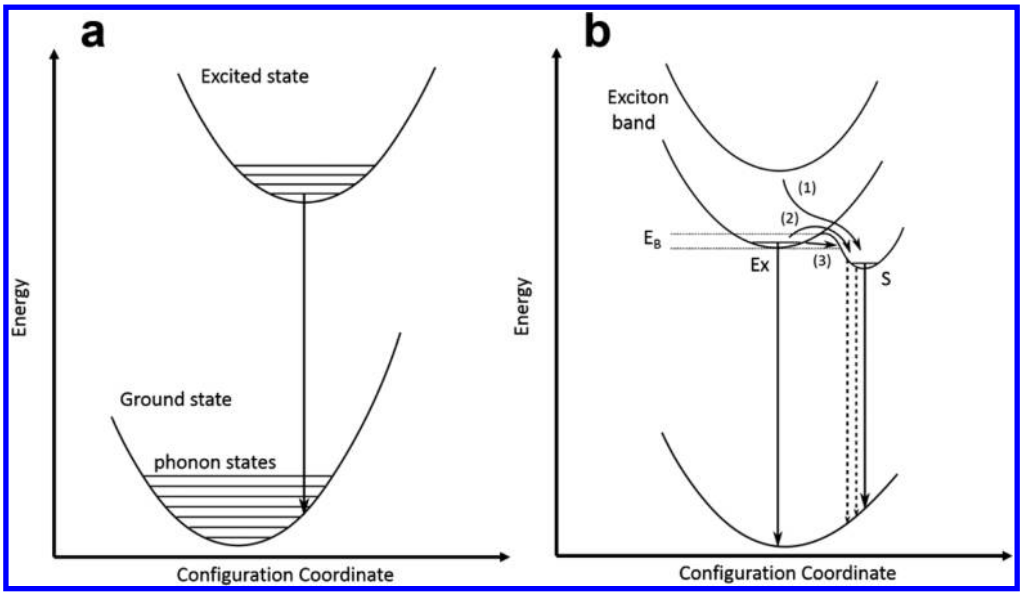

Figure 10. (a) An example of configuration coordinate diagram for a deep-level defect. (b) CC diagram illustrating the coexistence of free and self-trapping excitons. The letters Ex and S show the free and self-trapped states, respectively. Three distinct paths toward self-trapping are represented: direct relaxation (1), thermal overcoming of the barrier (2), and tunneling (3).

room temperature and should not be able to compete efficiently in the recombination process with the free excitonic emission. Consequently, one would expect to detect the free excitonic emission at room temperature. In the framework of self-trapping, the existence of an energy barrier in the adiabatic potential energy surface explains these unusual observations in a direct manner by the thermal overcoming of the barrier (Figure 10b). The quenching of the edge emission with an energy of 10−15 meV gives an order of magnitude of the energy barrier. This value is close to those reported for alkali-halide (e.g., KI 14−33 meV,[45] NaI 17 meV[46]).

In this hypothesis, the thermal evolution of the luminescence decay rate should be dominated by the thermal overcoming of the energy barrier process. The probability $1/\tau_{th} = \upsilon\, e^{-E/k_B T}$ for self-trapping by thermal transition includes the energy barrier, E (k_B is the Boltzmann constant) and the rate constant υ.[46,47] Hence, luminescence decay constants of Figure 8 have been fitted with the following law:

$$1/\tau = 1/\tau_0 + \upsilon\, e^{-E/k_B T} \quad (2)$$

with $1/\tau_0 = 1/\tau_r + 1/\tau_t$, where $1/\tau_t$ is the tunneling rate and $1/\tau_r$ is the transition probability by radiative recombination from

DOI: 10.1021/acs.jpcc.5b06211
J. Phys. Chem. C XXXX, XXX, XXX−XXX

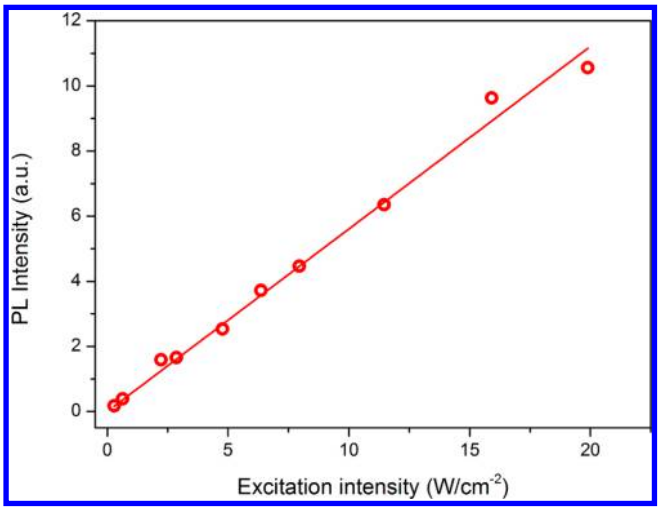

Figure 11. PL intensity of the WL band versus excitation power density.

the S state (Figure 10b). We have considered $1/\tau_0$ as relatively independent of temperature as compared to $1/\tau_{th}$. The results clearly indicate that the luminescence decay constants decrease exponentially with temperature as expected. Within this model, two energies were derived: $E_2 = 7.9 \pm 0.3$ meV and $E_1 = 11.5 \pm 0.6$ meV from the thermal evolution of τ_2 and τ_1. These values are close to those measured for the quenching of the free excitonic emission. The precise assignment of these two distinct energies is not straightforward, partly because we could not separate the WL1 and WL2 contributions.

Finally, we remarked previously that raising both the temperature and the excitation energy results in a relative increase in the WL1 emission. This very unusual behavior could be explained again in the framework of self-trapping. As stated previously, excitons created at high energy have the possibility to relax directly into the self-trapped state. Raising the excitation energy increases the direct relaxation path efficiency, while raising the temperature allows the thermal overcoming of the barrier (Figure 10b).

All of these experimental observations find a direct and consistent explanation with the hypothesis of self-trapped carriers. The WL1 and WL2 bands could correspond to excitons self-trapped on two different sites, with two distinct energy barriers. Another possibility is that the WL2 emission corresponds to a permanent trap state separated by an energy barrier from a self-trapped state (WL1 band), as described in the case of extrinsic self-trapping. Further investigations are needed, and particularly calculations of the electronic structure will be very helpful.

IV. CONCLUSIONS

We described the optical properties of white-light emission under UV irradiation in $(C_6H_{11}NH_3)_2PbBr_4$ thin films. The WL emission coexists at low temperature with an excitonic edge emission. Low-temperature optical absorption allows one to estimate the free exciton binding energy to 280 meV. However, the excitonic edge luminescence disappeared when the temperature was raised from 10 to 90 K, whereas the WL emission increases to reach a maximum. Heat capacity measurements and X-ray diffraction investigations did not show the presence of any first-order phase transition at the origin of this nonmonotonous thermal behavior. Time-resolved photoluminescence investigations show that the white luminescence decay time decreases exponentially with temperature in the same temperature range. Time-resolved absorption spectra demonstrate that the WL emission is composed of mainly two bands. The weight of these two bands in the overall emission changes with the temperature and excitation energy. Overall, the results find a straightforward explanation if we consider that the luminescence originates from self-trapped states and the existence of an energy barrier against self-trapping of approximately 10 meV.

■ ASSOCIATED CONTENT

Supporting Information

The Supporting Information is available free of charge on the ACS Publications website at DOI: 10.1021/acs.jpcc.5b06211.

Relevant structural parameters and reconstruction of the ($hk0$) layer of reciprocal space (PDF)

■ AUTHOR INFORMATION

Corresponding Authors

*E-mail: damien.garrot@uvsq.fr.
*E-mail: kbo@physique.uvsq.fr.

Notes

The authors declare no competing financial interest.

■ ACKNOWLEDGMENTS

This work was supported by the PHC MAGHREB program no. 13MAG08&30255ZJ, the "Agence Nationale de la Recherche" (ANR project BISTA-MAT: ANR-12-BS07-0030-01), Spanish MINECO (through the grant MAT2013-44063-R), Université de Versailles Saint-Quentin-En-Yvelines, CNRS, and Université de Sfax, which we deeply acknowledge.

■ REFERENCES

(1) Mitzi, D. B. Synthesis, structure, properties of organic-inorganic perovskites and related materials. *Prog. Inorg. Chem.* **1999**, *48*, 1−121.
(2) Papavassiliou, G.; Koutselas, I. Structural, optical and related properties of some natural 3-dimensional and lower-dimensional semiconductor systems. *Synth. Met.* **1995**, *71*, 1713−1714.
(3) Burschka, J.; Pellet, N.; Moon, S.-J.; Humphry-Baker, R.; Gao, P.; Nazeeruddin, M. K.; Graetzel, M. Sequential deposition as a route to high performance perovskite sensitized solar cells. *Nature* **2013**, *499*, 316−319.
(4) Kojima, A.; Teshima, K.; Shirai, Y.; Miyasaka, T. Organometal halide perovskites as visible-light sensitizers for photovoltaic cells. *J. Am. Chem. Soc.* **2009**, *131*, 6050−6051.
(5) Lee, M. M.; Teuscher, J.; Miyasaka, T.; Murakami, T. N.; Snaith, H. J. Efficient hybrid solar cells based on meso-superstructured organometal halide perovskites. *Science* **2012**, *338*, 643−647.
(6) Liu, M.; Johnston, M. B.; Snaith, H. J. Efficient planar heterojunction perovskite Solar cells by vapour deposition. *Nature* **2013**, *501*, 395−398.
(7) Zhou, H.; Chen, Q.; Li, G.; Luo, S.; Song, T.; Duan, H.-S.; Hong, Z.; You, J.; Liu, Y.; Yang, Y. Interface engineering of highly efficient perovskite solar cells. *Science* **2014**, *345*, 542−546.
(8) Xing, G.; Mathews, N.; Lim, S. S.; Yantara, N.; Liu, X.; Sabba, D.; Gratzel, M.; Mhaisalkar, S.; Sum, T. C. Low temperature solution-processed wavelength-tunable perovskites for lasing. *Nat. Mater.* **2014**, *13*, 476−480.
(9) Calabrese, J.; Jones, N. L.; Harlow, R. L.; Herron, N.; Thorn, D. L.; Wang, Y. Preparation and characterization of layered lead halide compounds. *J. Am. Chem. Soc.* **1991**, *113*, 2328−2330.
(10) Ishihara, T. Optical properties of PbI-based perovskite structures. *J. Lumin.* **1994**, *60−1*, 269−274.

DOI: 10.1021/acs.jpcc.5b06211
J. Phys. Chem. C XXXX, XXX, XXX−XXX

(11) Gauthron, K.; Lauret, J. S.; Doyennette, L.; Lanty, G.; Al Choueiry, A.; Zhang, S. J.; Brehier, A.; Largeau, L.; Mauguin, O.; Bloch, J.; et al. Optical spectroscopy of two-dimensional layered $(C_6H_5C_2H_4\text{-}NH_3)_2PbI_4$ perovskite. *Opt. Express* **2010**, *18*, 5912−5919.
(12) Ishihara, T.; Takahashi, J.; Goto, T. Optical properties due to electronic transitions in 2-dimensional semiconductors $(C_nH_{2n+1}NH_3)_2PbI_4$. *Phys. Rev. B: Condens. Matter Mater. Phys.* **1990**, *42*, 11099−11107.
(13) Era, M.; Morimoto, S.; Tsutsui, T.; Saito, S. Organic-inorganic heterostructure electroluminescent device using a layered perovskite semiconductor $(C_6H_5C_2H_4NH_3)_2PbI_4$. *Appl. Phys. Lett.* **1994**, *65*, 676−678.
(14) Hattori, T.; Taira, T.; Era, M.; Tsutsui, T.; Saito, S. Highly efficient electroluminescence from a heterostructure device combined with emissive layered-perovskite and an electron-transporting organic compound. *Chem. Phys. Lett.* **1996**, *254*, 103−108.
(15) Kagan, C. R.; Mitzi, D. B.; Dimitrakopoulos, C. D. Organic-inorganic hybrid materials as semiconducting channels in thin film field effect transistors. *Science* **1999**, *286*, 945−947.
(16) Brehier, A.; Parashkov, R.; Lauret, J. S.; Deleporte, E. Strong exciton-photon coupling in a microcavity containing layered perovskite semiconductors. *Appl. Phys. Lett.* **2006**, *89*, 171110.
(17) Lanty, G.; Zhang, S.; Lauret, J. S.; Deleporte, E.; Audebert, P.; Bouchoule, S.; Lafosse, X.; Zuñiga-Pérez, J.; Semond, F.; Lagarde, D.; et al. Hybrid cavity polaritons in a ZnO-perovskite microcavity. *Phys. Rev. B: Condens. Matter Mater. Phys.* **2011**, *84*, 195449.
(18) Braun, M.; Tuffentsammer, W.; Wachtel, H.; Wolf, H. C. Tailoring energy levels in lead chloride based layered perovskites and energy transfer between the organic and inorganic planes. *Chem. Phys. Lett.* **1999**, *303*, 157−164.
(19) Zhang, S. J.; Audebert, P.; Wei, Y.; Lauret, J. S.; Galmiche, L.; Deleporte, E. Synthesis and optical properties of novel organic-inorganic hybrid UV $(RNH_3)_2PbCl_4$ semiconductors. *J. Mater. Chem.* **2011**, *21*, 466−474.
(20) Zhang, S. J.; Lanty, G.; Lauret, J. S.; Deleporte, E.; Audebert, P.; Galmiche, L. Synthesis and optical properties of novel organic-inorganic hybrid nanolayer structure semiconductors. *Acta Mater.* **2009**, *57*, 3301−3309.
(21) Dohner, E. R.; Hoke, E. T.; Karunadasa, H. I. Self-Assembly broadband white-light emitters. *J. Am. Chem. Soc.* **2014**, *136*, 1718−1721.
(22) Dohner, E. R.; Jaffe, A.; Bradshaw, L. R.; Karunadasa, H. I. Intrinsic white light emission in layered hybrid perovskites. *J. Am. Chem. Soc.* **2014**, *136*, 13154−13157.
(23) Sheldrick, G. M. A short History of SHELX. *Acta Crystallogr., Sect. A: Found. Crystallogr.* **2008**, *64*, 112−122.
(24) CrysAlis CCD. *CrysAlis RED, version 171.37.31*; Oxford Diffraction: Wroclaw, Poland, 2014.
(25) Kitazawa, N.; Aono, M.; Watanabe, Y. Excitons in organic-inorganic hybrid compounds $(C_nH_{2n+1}NH_3)_2PbBr_4$ (n = 4, 5, 712). *Thin Solid Films* **2010**, *518*, 3199−3203.
(26) Kitazawa, N.; Watanabe, Y. Optical properties of natural quantum-well compounds $(C_6H_5\text{-}C_nH_{2n}\text{-}NH_3)_2PbBr_4$ (n = 1−4). *J. Phys. Chem. Solids* **2010**, *71*, 797−802.
(27) Reshchikov, M.; Morkoc, H. Luminescence properties of defects in GaN. *J. Appl. Phys.* **2005**, *97*, 061301.
(28) Tanaka, K.; Takahashi, T.; Kondo, T.; Umeda, K.; Ema, K.; Umebayashi, T.; Asai, K.; Uchida, K.; Miura, N. Electronic and excitonic structures of inorganic-organic perovskite-type quantum-well crystal $(C_4H_9NH_3)_2$ $PbBr_4$. *Jpn. J. Appl. Phys.* **2005**, *44*, 5923−5932.
(29) Kitazawa, N.; Aono, M.; Watanabe, Y. Temperature-dependent time-resolved photoluminescence of $(C_6H_5C_2H_4NH_3)_2PbX_4$ (X = Br, I). *Mater. Chem. Phys.* **2012**, *134*, 875−880.
(30) Jiang, D.; Jung, H.; Ploog, K. Temperature-dependence of photoluminescence from GaAs single and multiple quantum-well heterostructures grown by molecular-beam epitaxy. *J. Appl. Phys.* **1988**, *64*, 1371−1377.
(31) Billing, D. G.; Lemmerer, A. Synthesis, characterization and phase transitions of the inorganic-organic layered perovskite-type hybrids $[(C_nH_{2n+1}NH_3)_2PbI_4]$ (n = 12, 14, 16 and 18). *New J. Chem.* **2008**, *32*, 1736−1746.
(32) Billing, D. G.; Lemmerer, A. Synthesis, characterization and phase transitions in the inorganic-organic layered perovskite-type hybrids $[(C_nH_{2n+1}NH_3)_2PbI_4]$, n = 4, 5 and 6. *Acta Crystallogr., Sect. B: Struct. Sci.* **2007**, *63*, 735−747.
(33) Onoda-Yamamuro, N.; Matsuo, T.; Suga, H. Calorimetric and IR Spectroscopic Studies of Phase Transitions in Methylammonium Trihalogenoplumbates. *J. Phys. Chem. Solids* **1990**, *51*, 1383−1395.
(34) Koubaa, M.; Dammak, T.; Garrot, D.; Castro, M.; Codjovi, E.; Mlayah, A.; Abid, Y.; Boukheddaden, K. Thermally-induced first-order phase transition in the $(FC_6H_4C_2H_4NH_3)_2[PbI_4]$ photoluminescent organic-inorganic material. *J. Appl. Phys.* **2012**, *111*, 053521.
(35) Pradeesh, K.; Baumberg, J. J.; Prakash, G. V. Temperature-induced exciton switching in long alkyl chain based inorganic-organic hybrids. *J. Appl. Phys.* **2012**, *111*, 013511.
(36) Billing, D. G.; Lemmerer, A. Inorganic-organic hybrid materials incorporating primary cyclic ammonium cations: The lead bromide and chloride series. *CrystEngComm* **2009**, *11*, 1549−1562.
(37) McCluskey, M. D.; Jokela, S. J. Defects in ZnO. *J. Appl. Phys.* **2009**, *106*, 071101.
(38) Fugol, I. Excitons in rare gas crystals. *Adv. Phys.* **1978**, *27*, 1−87.
(39) Plekhanov, V. Lead halides: Electronic properties applications. *Prog. Mater. Sci.* **2004**, *49*, 787−886.
(40) Toyozawa, Y. Self-trapping of an electron by the acoustical mode of lattice vibration.1. *Prog. Theor. Phys.* **1961**, *26*, 29−44.
(41) Williams, R.; Song, K. The self-trapped exciton. *J. Phys. Chem. Solids* **1990**, *51*, 679−716.
(42) Iwanaga, M.; Hayashi, T. Exciton-relaxation dynamics in lead halides. *J. Lumin.* **2003**, *102*, 663−668.
(43) Lushchik, A.; Kirm, M.; Lushchik, C.; Martinson, I.; Zimmerer, G. Luminescence of free and self-trapped excitons in wide-gap oxides. *J. Lumin.* **2000**, *87*−*89*, 232−234.
(44) Stoneham, A. M.; Gavartin, J.; Shluger, A. L.; Kimmel, A. V.; Ramo, D. M.; Ronnow, H. M.; Aeppli, G.; Renner, C. Trapping, self-trapping and the polaron family. *J. Phys.: Condens. Matter* **2007**, *19*, 255208.
(45) Vankhiem, T.; Nouailhat, A. The Free Exciton In KI. II. Coexistence With The Self-Trapped Exciton. *J. Phys. Soc. Jpn.* **1981**, *50*, 127−128.
(46) Nishimura, H.; Ohhigashi, C.; Tanaka, Y.; Tomura, M. Resonance luminescence lines of of free excitons in alkali iodide single-crystals. *J. Phys. Soc. Jpn.* **1977**, *43*, 157−163.
(47) Matsui, A.; Mizuno, K.; Tamai, N.; Yamazaki, I. Transient free-exciton luminescence and exciton-lattice interaction in pyrene crystals. *Chem. Phys.* **1987**, *113*, 111−117.

DOI: 10.1021/acs.jpcc.5b06211
J. Phys. Chem. C XXXX, XXX, XXX−XXX